Statistical Performance Analysis of Signal Variance-Based Dipole Models for MEG/EEG Source Localization and Detection

Alberto Rodríguez-Rivera*, *Student Member, IEEE*, Barry D. Van Veen, *Fellow, IEEE*, and Ronald T. Wakai

***Abstract*—A set of dipole fitting algorithms that incorporate different assumptions about the variability of the signal component into their mathematical models is presented and analyzed. Dipole fitting is performed by minimizing the squared error between the selected data model and available data. Dipole models based on moments that have 1) constant amplitude and orientation, 2) variable amplitude and fixed known orientation, 3) variable amplitude and fixed unknown orientation, and 4) variable amplitude and variable orientation are considered. The presence of a dipolar source is determined by comparing the fractional energy explained by the dipole model to a threshold. Source localization is accomplished by searching to find the location that explains the largest fractional signal energy using a dipole model. Expressions for the probability of a false positive decision and probability of correct detection are derived and used to evaluate the effect of variability in the dipole on performance and to address the effects of model mismatch and location errors. Simulated and measured data experiments are presented to illustrate the performance of both detection and localization methods. The results indicate that models which account for variance outperform the constant orientation and magnitude model even when the number of observations is relatively small and the signal of interest contains a very modest variance component.**

***Index Terms*—Evoked experiments, hypothesis testing, MEG/EEG, parameter estimation, signal detection, signal related variance, source localization.**

I. Introduction

LEAST squares dipole fitting is commonly used to detect the presence of a dipolar source, and to identify the location of the source. In this paper we consider the problem of detecting and localizing a dipolar source given multiple independent observations or trials of the same underlying phenomenon at a single instant in time. For example, given multiple evoked responses, we consider localizing a peak in the response such as the N100, or localizing the peaks of several epileptic spikes. We consider four different models for the dipolar source across trials: 1) constant unknown dipole moment; 2) fixed, known moment orientation with variable unknown amplitude; 3) fixed unknown moment orientation with variable unknown amplitude; and 4) variable unknown moment amplitude and orientation. The last three models explicitly capture variability in an event across multiple trials. Analogous models have been used to capture temporal evolution; see for example Mosher *et al.* [1].

Randomness or variability in MEG and EEG spatio–temporal data is often identified as noise and treated accordingly. For example, averaging is often employed to reduce the effects of nonrepeatable events. However, there is important information in unaveraged event-related MEG/EEG data, as noted in Baillet, *et al.* [2]. For example, averaging destroys noninterlocked synchronization signals between long distance cells [3]. Averaging also reduces the effective SNR when signal related variance is present. Signal related variance arises naturally in MEG/EEG evoked experiments from:

- trial to trial variations in response amplitude;
- trial to trial variations in latency;
- sources generating signals with different temporal morphology but originating from the same spatial location.

Amplitude changes are common because the biochemical state of neurons may change from trial to trial. Latency jitter is common in neuromagnetic and neuroelectric evoked response experiments and is difficult to remove when a template of the response is not available. Spontaneous activity such as epileptic spikes are also difficult to synchronize due to differences in spike duration and morphology.

Localization algorithms, such as Linearly Constrained Minimum Variance (LCMV) spatial filtering [4], Multiple Signal Classification (MUSIC) [1] and weighted MUSIC [5], exploit variance through their reliance on the covariance matrix of the data. The covariance matrix represents both signal and noise variance; thus, covariance matrix-based algorithms only indirectly exploit signal variance. Furthermore, a relatively large number of independent data observations are required to obtain an acceptable estimate of the true covariance matrix. For example, LCMV-based algorithms require the number of data observations to exceed the number of channels by a factor of at least three to five in order to obtain statistically stable results [4], [6]. Hence, covariance matrix based algorithms are limited to applications in which a relatively large number of observations are available. Increasing interest in the study of scenarios characterized by limited data [2], [3], [7], and [8] motivates the development and analysis of localization and event detection algorithms that both exploit variance and operate with relatively small numbers of observations, such as those described in this paper.

Manuscript received March 14, 2002; revised August 31, 2002. This work was supported by the Public Health Services under Grant R01 HL63174. *Asterisk indicates corresponding author.*

*A. Rodríguez-Rivera is with the Department of Electrical and Computer Engineering, University of Wisconsin-Madison, 1415 Engineering Dr., Madison, WI 53706 USA (e-mail: arod@ieee.org).

B. D. Van Veen is with the Department of Electrical and Computer Engineering, University of Wisconsin-Madison, Madison, WI 53706 USA.

R. T. Wakai is with the Department of Medical Physics, University of Wisconsin, Madison WI 53706 USA.

Digital Object Identifier 10.1109/TBME.2002.807661

Dipole fitting is accomplished by choosing the model parameters to minimize the squared error between the dipole model and the data. The fractional energy explained by the model defines a goodness of fit metric that is used for detecting the presence of a source and localizing the source. A statistical analysis of the goodness of fit metric is presented in this paper to guide the selection of a threshold for determining whether the dipole model is appropriate, to determine the likelihood of correctly identifying an actual dipole, and to analyze the effects of location errors and model mismatch. The performance depends on the dimensional parameters of the problem, a signal to noise ratio that is defined in terms of the second moment of the signal, and a loss factor associated with location error and model mismatch. Detection and localization performance is verified using simulated and epileptic spike data. We conclude that dipole models based on variability generally offer much better performance than the constant dipole moment model, even when the actual signal variability is very small.

The paper is structured in the following manner. Section II presents the mathematical models and goodness of fit metrics for each dipole fitting algorithm. In Section III we derive the test statistics for the performance metrics, obtain their probability density functions, and derive expressions for the probability of false positive decisions and the probability of correctly detecting a source. We also analyze the effect of using the wrong model and two metrics of localization performance. Section IV presents several examples to demonstrate the effectiveness of the approach followed by comments and conclusions.

Lower- and upper-case bold face symbols represent column vectors and matrices while superscript t and -1 denote matrix transpose and inverse, respectively. The trace of a matrix $\mathbf{A}$ is written as $\mathrm{tr}\{\mathbf{A}\}$ and the symbol $\mathbf{I}_p$ denotes the $p \times p$ identity matrix.

II. Dipole Fitting Algorithms

The detection and source localization algorithms discussed in this paper are based on mathematical models that relate the underlying neural activity to the distribution of the electromagnetic field strength or electric field potentials measured outside the human body. This section develops these models and provides the basic performance structure by which the proposed algorithms are judged. We assume biomagnetic data throughout the paper, although the analysis and conclusions are directly applicable to bioelectric or joint data.

Let $\mathbf{x}(i)$ be a vector of size $N \times 1$ representing the ith magnetic field strength measurement at N selected sensor sites, where the index i represents the event or epoch number, that is, a distinct observation of the same underlying phenomenon. We assume one active source, modeled as an equivalent current dipole [2] at an unknown location represented by the 3×1 vector $\boldsymbol{\theta}$. The data may be modeled as

$$\mathbf{x}(i) = \mathbf{H}(\boldsymbol{\theta})\tilde{\mathbf{m}}(i) + \mathbf{n}(i) \tag{1}$$

where the $N \times 3$ matrix $\mathbf{H}(\boldsymbol{\theta})$ is a matrix whose columns represent the magnetic field strength generated by unit dipoles pointing in the x, y and z directions, respectively, at location $\boldsymbol{\theta}$, the 3×1 vector $\tilde{\mathbf{m}}(i)$ represents the moment of the equivalent current dipole, and $\mathbf{n}(i)$ represents noise. In the analysis that follows we assume the noise is uncorrelated over the event index i, that is, $E\{\mathbf{n}(i)\mathbf{n}^t(j)\} = \mathbf{0}$ for $i \neq j$. This assumption is not generally true if the data represents a time series. Note that we assume the source location $\boldsymbol{\theta}$ is unknown, but fixed for all observations.

The three columns of the forward transfer matrix $\mathbf{H}(\boldsymbol{\theta})$ define a set of three basis vectors that span the component of the data associated with the dipole at $\boldsymbol{\theta}$. In the magnetic case the external field strength generated by radially oriented dipoles outside a spherically symmetric volume conductor is zero, so our assumption of a spherically symmetric head model forces $\mathbf{H}(\boldsymbol{\theta})$ to be rank two.[1] To simplify the later analysis we generate a two dimensional orthogonal basis for the space spanned by $\mathbf{H}(\boldsymbol{\theta})$. Decompose $\mathbf{H}(\boldsymbol{\theta})$ as the product of an $N \times 2$ matrix $\mathbf{U}(\boldsymbol{\theta})$ having orthogonal columns and a 2×3 matrix $\mathbf{R}(\boldsymbol{\theta})$, that is $\mathbf{H}(\boldsymbol{\theta}) = \mathbf{U}(\boldsymbol{\theta})\mathbf{R}(\boldsymbol{\theta})$. We rewrite the signal model in terms of the orthogonal basis vectors as

$$\mathbf{x}(i) = \mathbf{U}(\boldsymbol{\theta})\mathbf{m}(i) + \mathbf{n}(i) \tag{2}$$

where the 2×1 vector $\mathbf{m}(i) = \mathbf{R}(\boldsymbol{\theta})\tilde{\mathbf{m}}(i)$ is the transformed dipole moment. Notice that while this transformation is mathematically convenient, the transformed dipole moment no longer corresponds to a physical dipole moment. For notational clarity we ignore the dependence of the transformed moment $\mathbf{m}(i)$ on $\boldsymbol{\theta}$.

The four dipole models considered in this paper are as follows.

1) Constant unknown dipole moment: $\mathbf{m}(i) = \mathbf{m}_m$.
2) Fixed known dipole moment orientation, variable moment amplitude: $\mathbf{m}(i) = \mathbf{m}_o g(i)$, where $\mathbf{m}_o$ is known and unit norm, $\mathbf{m}_o^t\mathbf{m}_o = 1$.
3) Fixed unknown dipole moment orientation, variable moment amplitude: $\mathbf{m}(i) = \mathbf{m}_o g(i)$, where $\mathbf{m}_o$ is unit norm.
4) Variable dipole moment orientation and magnitude: $\mathbf{m}(i)$.

It has been suggested that evoked response experiments fall under the fixed dipole moment orientation category, while spontaneous epileptic data is better described by a variable moment orientation [9]. Mosher, *et al.* [1] refer to the first two models as "fixed location and orientation" and the third as "fixed location unconstrained orientation" when fitting the temporal evolution of a source.

In each case the unknown model parameters are obtained by minimizing the squared error between the data and the model, expressed in general as

$$E^2(\boldsymbol{\theta}) = \sum_{i=1}^{L} ||\mathbf{x}(i) - \mathbf{U}(\boldsymbol{\theta})\mathbf{m}(i)||^2. \tag{3}$$

Minimizing the squared error maximizes the fractional energy explained by the corresponding dipole model, or the goodness of fit. Although this approach may appear *ad hoc*, it can be shown that equivalent test statistics are obtained using the well-known generalized likelihood ratio test [10] (GLRT) procedure

[1]The case where $\mathbf{H}(\boldsymbol{\theta})$ is full rank will only introduce a dimensional change to the analysis that follows.

assuming the noise $\mathbf{n}(i)$ is zero-mean Gaussian with covariance $\sigma^2\mathbf{I}$, where σ^2 is unknown. Depending on the assumed dipole model, the goodness of fit may be a function of location or dipole orientation.

A. Constant Dipole Model

Assume the dipole moment $\mathbf{m}(i) = \mathbf{m}_m$ is fixed. Substitute $\mathbf{m}(i) = \mathbf{m}_m$ into (3) to obtain the minimum mean squared error dipole moment estimate

$$\hat{\mathbf{m}}_m = \mathbf{U}^t(\boldsymbol{\theta})\overline{\mathbf{x}} \tag{4}$$

where

$$\overline{\mathbf{x}} = \frac{1}{L}\sum_{i=1}^{L}\mathbf{x}(i) \tag{5}$$

is the mean, or average data vector. Note that we have used $\mathbf{U}^t(\boldsymbol{\theta})\mathbf{U}(\boldsymbol{\theta}) = \mathbf{I_2}$ in deriving (4).

The goodness of fit expressed as a function of $\boldsymbol{\theta}$ and $\hat{\mathbf{m}}_m$ is

$$GF_m(\boldsymbol{\theta}, \hat{\mathbf{m}}_m) = 1 - \frac{|\mathbf{U}(\boldsymbol{\theta})\hat{\mathbf{m}}_m - \overline{\mathbf{x}}|^2}{|\overline{\mathbf{x}}|^2}. \tag{6}$$

Substitute the estimate $\hat{\mathbf{m}}_m$ from (4) into (6) to obtain

$$GF_m(\boldsymbol{\theta}) = \frac{\overline{\mathbf{x}}^t\mathbf{U}(\boldsymbol{\theta})\mathbf{U}^t(\boldsymbol{\theta})\overline{\mathbf{x}}}{\overline{\mathbf{x}}^t\overline{\mathbf{x}}}. \tag{7}$$

A location estimate $\hat{\boldsymbol{\theta}}$ is obtained by maximizing $GF(\boldsymbol{\theta})$ over all $\boldsymbol{\theta}$. The numerator of $GF_m(\boldsymbol{\theta})$ is the energy in the projection of the mean onto the space spanned by the forward transfer matrix $\mathbf{U}(\boldsymbol{\theta})$. Hence, the goodness of fit is the fraction of the energy in the mean that lies in the space spanned by $\mathbf{U}(\boldsymbol{\theta})$.

B. Fixed Known Dipole Orientation

Here we assume a fixed *known* dipole orientation $\mathbf{m}_o$ so that $\mathbf{m}(i) = \mathbf{m}_o g(i)$ and variable dipole magnitude $g(i)$. The goal is to find $g(i)$ so as to minimize (3), which gives

$$\hat{g}(i) = \mathbf{m}_o^t\mathbf{U}^t(\boldsymbol{\theta})\mathbf{x}(i). \tag{8}$$

Define the unit length vector $\mathbf{v}(\boldsymbol{\theta}) = \mathbf{U}(\boldsymbol{\theta})\mathbf{m}_o$. The vector $\mathbf{v}(\boldsymbol{\theta})$ is the expected spatial pattern generated by a unit strength dipolar source with transformed moment $\mathbf{m}_o$ so that $\hat{g}(i) = \mathbf{v}^t(\boldsymbol{\theta})\mathbf{x}(i)$. The corresponding goodness of fit is expressed as

$$GF_f(\boldsymbol{\theta}) = \frac{\sum_{i=1}^{L}\mathbf{x}^t(i)\mathbf{v}(\boldsymbol{\theta})\mathbf{v}^t(\boldsymbol{\theta})\mathbf{x}(i)}{\sum_{i=1}^{L}\mathbf{x}^t(i)\mathbf{x}(i)}. \tag{9}$$

Note that $\mathbf{x}^t(i)\mathbf{v}(\boldsymbol{\theta})\mathbf{v}^t(\boldsymbol{\theta})\mathbf{x}(i) = \hat{g}^2(i)$ is the magnitude squared of the projection of $\mathbf{x}(i)$ onto the space spanned by $\mathbf{v}(\boldsymbol{\theta})$. Hence, $GF_f(\boldsymbol{\theta})$ is the fraction of the energy in the data that is consistent with $\mathbf{v}(\boldsymbol{\theta})$, the expected spatial pattern for a source at $\boldsymbol{\theta}$. Apply the identity $\mathbf{a}^t\mathbf{b} = \mathrm{tr}(\mathbf{b}\mathbf{a}^t)$ to rewrite (9) as

$$GF_f(\boldsymbol{\theta}) = \frac{\sum_{i=1}^{L}\hat{g}^2(i)}{\mathrm{tr}(\mathbf{S})} \tag{10}$$

where $\mathbf{S} = \sum_{i=1}^{L}\mathbf{x}(i)\mathbf{x}^t(i)$ is the sample correlation matrix. The kth element on the main diagonal of $\mathbf{S}$ is the energy in the kth channel so $\mathrm{tr}(\mathbf{S})$ is the total energy in all channels. The goodness of fit is, thus, the ratio of energy in the signal component of the data to the total energy.

C. Fixed Unknown Dipole Orientation

Here, we use $\mathbf{m}(i) = \mathbf{m}_o g(i)$ where $\mathbf{m}_o$ is unit length but unknown. The goal is to find the dipole orientation $\mathbf{m}_o$ and amplitude $g(i)$ that minimizes the squared error given by (3). First, we minimize with respect to $g(i)$ as in (8). Use $\mathbf{m}_o^t\mathbf{m}_o = 1$ to obtain an estimate of $g(i)$ as a function of the unknown $\mathbf{m}_o$

$$\hat{g}(i) = \mathbf{m}_o^t\mathbf{U}^t(\boldsymbol{\theta})\mathbf{x}(i). \tag{11}$$

Now the problem is to solve for the $\mathbf{m}_o$ that satisfies

$$\min_{\mathbf{m}_o}\left\{\sum_{i=1}^{L}|\mathbf{x}(i) - \mathbf{U}(\boldsymbol{\theta})\mathbf{m}_o\mathbf{m}_o^t\mathbf{U}^t(\boldsymbol{\theta})\mathbf{x}(i)|^2\right\} \quad \text{s.t. } \|\mathbf{m}_o\|^2 = 1. \tag{12}$$

The minimization problem (12) may be rewritten as

$$\min_{\mathbf{m}_o}\left\{\sum_{i=1}^{L}\mathbf{x}^t(i)(\mathbf{I}_N - \mathbf{U}(\boldsymbol{\theta})\mathbf{m}_o\mathbf{m}_o^t\mathbf{U}^t(\boldsymbol{\theta}))\mathbf{x}(i)\right\} \quad \text{s.t. } \|\mathbf{m}_o\|^2 = 1 \tag{13}$$

which is equivalent to the maximization problem

$$\max_{\mathbf{m}_o}\left\{\sum_{i=1}^{L}|\mathbf{x}^t(i)\mathbf{U}(\boldsymbol{\theta})\mathbf{m}_o|^2\right\} \quad \text{s.t. } \|\mathbf{m}_o\|^2 = 1 \tag{14}$$

or

$$\max_{\mathbf{m}_o}\{\mathbf{m}_o^t\mathbf{U}^t(\boldsymbol{\theta})\mathbf{S}\mathbf{U}(\boldsymbol{\theta})\mathbf{m}_o\} \quad \text{s.t. } \|\mathbf{m}_o\|^2 = 1. \tag{15}$$

The solution to the Rayleigh quotient represented by (15) is obtained by choosing $\hat{\mathbf{m}}_o$ as the eigenvector corresponding to the maximum eigenvalue of $\mathbf{U}^t(\boldsymbol{\theta})\mathbf{S}\mathbf{U}(\boldsymbol{\theta})$ [11], that is

$$\hat{\mathbf{m}}_o(\boldsymbol{\theta}) = \max \text{ eigenvector} \quad \{\mathbf{U}^t(\boldsymbol{\theta})\mathbf{S}\mathbf{U}(\boldsymbol{\theta})\}. \tag{16}$$

The optimum moment orientation $\hat{\mathbf{m}}_o$ is, thus, a function of source location $\boldsymbol{\theta}$.

The goodness of fit is, thus, expressed as

$$GF_u(\boldsymbol{\theta}) = \frac{\sum_{i=1}^{L}\mathbf{x}^t(i)\mathbf{v}(\boldsymbol{\theta})\mathbf{v}^t(\boldsymbol{\theta})\mathbf{x}(i)}{\sum_{i=1}^{L}\mathbf{x}^t(i)\mathbf{x}(i)} \tag{17}$$

where $\mathbf{v}(\boldsymbol{\theta}) = \mathbf{U}(\boldsymbol{\theta})\hat{\mathbf{m}}_o(\boldsymbol{\theta})$. Again using $\mathbf{a}^t\mathbf{b} = \mathrm{tr}(\mathbf{b}\mathbf{a}^t)$ we may rewrite (17) as

$$GF_u(\boldsymbol{\theta}) = \frac{\lambda_{\max}(\boldsymbol{\theta})}{\mathrm{tr}(\mathbf{S})} \tag{18}$$

where $\lambda_{\max}(\boldsymbol{\theta}) = \hat{\mathbf{m}}_o^t(\boldsymbol{\theta})\mathbf{U}^t(\boldsymbol{\theta})\mathbf{S}\mathbf{U}(\boldsymbol{\theta})\hat{\mathbf{m}}_o(\boldsymbol{\theta})$ is the maximum eigenvalue of $\mathbf{U}^t(\boldsymbol{\theta})\mathbf{S}\mathbf{U}(\boldsymbol{\theta})$. The quantity $\lambda_{\max}(\boldsymbol{\theta})$ is the maximum energy in any one dimension of the space spanned by

$$\{\mathbf{U}(\boldsymbol{\theta})\mathbf{x}(i),\ i = 1, 2, \ldots, L\}. \tag{19}$$

Note that the numerator of $GF_f(\boldsymbol{\theta})$ has the form $\mathbf{m}_o^t\mathbf{U}^t(\boldsymbol{\theta})\mathbf{S}\mathbf{U}(\boldsymbol{\theta})\mathbf{m}_o$. Since $\lambda_{\max}(\boldsymbol{\theta}) \geq \mathbf{m}_o^t\mathbf{U}^t(\boldsymbol{\theta})\mathbf{S}\mathbf{U}(\boldsymbol{\theta})\mathbf{m}_o$ we know that $GF_u(\boldsymbol{\theta}) \geq GF_f(\boldsymbol{\theta})$. The additional flexibility afforded by an unknown moment orientation cannot decrease the goodness of fit relative to the fixed orientation case.

D. Variable Dipole Moment Orientation and Amplitude

In the most general case the dipole moment orientation and amplitude varies across the observations. Minimizing the squared modeling error in (3) with respect to the moment $\mathbf{m}(i)$ yields

$$\hat{\mathbf{m}}(i) = \mathbf{U}^t(\boldsymbol{\theta})\mathbf{x}(i). \tag{20}$$

Hence, the goodness of fit is

$$GF_r(\boldsymbol{\theta}) = \frac{\sum_{i=1}^{L}\mathbf{x}^t(i)\mathbf{U}(\boldsymbol{\theta})\mathbf{U}^t(\boldsymbol{\theta})\mathbf{x}(i)}{\sum_{i=1}^{L}\mathbf{x}^t(i)\mathbf{x}(i)} \tag{21}$$

$$= \frac{\mathrm{tr}(\mathbf{U}^t(\boldsymbol{\theta})\mathbf{S}\mathbf{U}(\boldsymbol{\theta}))}{\mathrm{tr}(\mathbf{S})}. \tag{22}$$

Here, we see that the goodness of fit is the ratio of the energy in the space spanned by the columns of $\mathbf{U}(\boldsymbol{\theta})$ to the total energy. Since $\mathbf{U}^t(\boldsymbol{\theta})\mathbf{S}\mathbf{U}(\boldsymbol{\theta})$ has two nonnegative eigenvalues and the trace of a matrix is the sum of its eigenvalues, we see that $\lambda_{\max}(\boldsymbol{\theta}) \leq \mathrm{tr}(\mathbf{U}^t(\boldsymbol{\theta})\mathbf{S}\mathbf{U}(\boldsymbol{\theta}))$ and, thus

$$GF_r(\boldsymbol{\theta}) \geq GF_u(\boldsymbol{\theta}) \geq GF_f(\boldsymbol{\theta}). \tag{23}$$

This is consistent with our intuition, since the more flexible model should be able to obtain a better fit to the data.

III. Statistical Analysis of Performance

The dipole fitting algorithms described in the previous section may be used to determine the presence or absence of a dipolar source by comparing the goodness of fit to a threshold. Localization is accomplished by finding the value $\boldsymbol{\theta}$ that maximizes the goodness of fit. In this section we derive the probability of incorrectly deciding a dipolar source is present given that the data consists of noise (a quantity also called the probability of a false positive decision) and the probability of correctly deciding a dipolar source is present (a quantity also called the probability of detection). We also examine the localization performance.

A fair comparison of different detection algorithms is performed by evaluating the probabilities of detection assuming that each algorithm has equal probability of false positive decisions. The probability of false positive (FP) decision is given by the expression

$$P_{\mathrm{FP}} = \int_{\beta}^{\infty} f_n(G)\,dG \tag{24}$$

where β is the test threshold, G represents the goodness of fit, and $f_n(G)$ is the probability density function of the goodness of fit assuming the data consists of noise. Similarly, the probability of detection is given by

$$P_D = \int_{\beta}^{\infty} f_p(G)\,dG \tag{25}$$

where $f_p(G)$ is the probability density function of the goodness of fit assuming a dipolar source is present. We shall show that P_{FP} is a function of only the threshold β and the dimensional parameters of the problem, and that it does not depend on the noise variance. P_D, however, depends in general on the dimensional parameters, the threshold β, a quantity we identify as the signal to noise ratio, and the mismatch between the true source location and the test location.

The noise $\mathbf{n}(i)$ in (2) is assumed zero mean, independent and identically Gaussian distributed across channels with $E\{\mathbf{n}(i)\mathbf{n}^t(i)\} = \sigma^2\mathbf{I}_N$ so we write

$$\mathbf{n}(i) \sim N(\mathbf{0},\ \sigma^2\mathbf{I}_N). \tag{26}$$

Recall that we also assume that noise is independent over the event index i. The signal component contributes a changing mean to the data and, thus

$$\mathbf{x}(i) \sim N(\mathbf{U}(\boldsymbol{\theta})\mathbf{m}(i),\ \sigma^2\mathbf{I}_N). \tag{27}$$

For convenience and without loss of generality we analyze a monotonic function of the goodness of fit

$$T(\boldsymbol{\theta}) = \frac{GF(\boldsymbol{\theta})}{1 - GF(\boldsymbol{\theta})}. \tag{28}$$

The test for the presence of a dipole at $\boldsymbol{\theta}$ is then expressed as

$$T(\boldsymbol{\theta}) \underset{\text{nodipole}}{\overset{\text{dipole}}{\gtrless}} \frac{\beta}{1-\beta}. \tag{29}$$

We now show that $T(\boldsymbol{\theta})$ is an F-distributed random variable in all cases.

A. Constant Dipole Model

Let $\mathbf{U}_{\perp}(\boldsymbol{\theta})$ be an $N \times N-2$ matrix whose columns form an orthonormal basis for the space orthogonal to that spanned by the columns of $\mathbf{U}(\boldsymbol{\theta})$. Consequently,

$$\mathbf{U}(\boldsymbol{\theta})\mathbf{U}^t(\boldsymbol{\theta}) + \mathbf{U}_{\perp}(\boldsymbol{\theta})\mathbf{U}_{\perp}^t(\boldsymbol{\theta}) = \mathbf{I}_N. \tag{30}$$

Using this identity and transforming the constant dipole fitting test (7) according to (28) we obtain

$$T_m(\boldsymbol{\theta}) = \frac{\overline{\mathbf{x}}^t\mathbf{U}(\boldsymbol{\theta})\mathbf{U}^t(\boldsymbol{\theta})\overline{\mathbf{x}}}{\overline{\mathbf{x}}^t\mathbf{U}_{\perp}(\boldsymbol{\theta})\mathbf{U}_{\perp}^t(\boldsymbol{\theta})\overline{\mathbf{x}}} \underset{\text{no dipole}}{\overset{\text{dipole}}{\gtrless}} \frac{\beta_m}{1-\beta_m} \tag{31}$$

where β_m is the goodness of fit test threshold, and $T_m(\boldsymbol{\theta})$ represents the ratio of the energy of the mean in the space spanned by the columns of $\mathbf{U}(\boldsymbol{\theta})$ to that outside the same space.

We first determine P_{FP_m} by computing the density of $T_m(\boldsymbol{\theta})$ assuming $\mathbf{x}(i) = \mathbf{n}(i)$. In this case,

$\overline{\mathbf{x}} \sim N(\mathbf{0}, (\sigma^2/L)\mathbf{I}_N)$ and $\mathbf{U}^t(\boldsymbol{\theta})\overline{\mathbf{x}} \sim N(\mathbf{0}, (\sigma^2/L)\mathbf{I}_2)$. Similarly, $\mathbf{U}_\perp^t(\boldsymbol{\theta})\overline{\mathbf{x}} \sim N(\mathbf{0}, (\sigma^2/L)\mathbf{I}_{N-2})$. The elements $\mathbf{U}^t(\boldsymbol{\theta})\overline{\mathbf{x}}$ and $\mathbf{U}_\perp^t(\boldsymbol{\theta})\overline{\mathbf{x}}$ are statistically independent because $\mathbf{U}(\boldsymbol{\theta})$ and $\mathbf{U}_\perp(\boldsymbol{\theta})$ are orthogonal. Furthermore, since $\overline{\mathbf{x}}^t\mathbf{U}(\boldsymbol{\theta})\mathbf{U}^t(\boldsymbol{\theta})\overline{\mathbf{x}}$ and $\overline{\mathbf{x}}^t\mathbf{U}_\perp(\boldsymbol{\theta})\mathbf{U}_\perp^t(\boldsymbol{\theta})\overline{\mathbf{x}}$ are sums of squares of independent identically distributed zero-mean Gaussian random variables, we have [12]

$$\frac{L}{\sigma^2}\,\overline{\mathbf{x}}^t\mathbf{U}(\boldsymbol{\theta})\mathbf{U}^t(\boldsymbol{\theta})\overline{\mathbf{x}} \sim \chi_2^2 \tag{32}$$

and

$$\frac{L}{\sigma^2}\,\overline{\mathbf{x}}^t\mathbf{U}_\perp(\boldsymbol{\theta})\mathbf{U}_\perp^t(\boldsymbol{\theta})\overline{\mathbf{x}} \sim \chi_{N-2}^2 \tag{33}$$

are central Chi-squared random variables with 2 and $N-2$ degrees of freedom, respectively. The ratio of independent Chi-squared random variables is F-distributed [12], so we have

$$\frac{N-2}{2}\,T_m(\boldsymbol{\theta}) = F_{2,\,N-2} \tag{34}$$

and the probability of a false positive decision is

$$P_{\mathrm{FP}_m} = \int_{t_m}^{\infty} F_{2,\,N-2}(T_m)\,dT_m \tag{35}$$

where

$$t_m = \left(\frac{\beta_m}{1-\beta_m}\right)\left(\frac{N-2}{2}\right). \tag{36}$$

Notice that the probability of a false positive decision depends only on the threshold β_m and dimensional parameters of the problem. Thus, we may choose the threshold to set P_{FP_m} without any additional knowledge.

To determine the probability of detection, we assume the true source location is $\boldsymbol{\theta}'$. In this case $\mathbf{U}^t(\boldsymbol{\theta})\overline{\mathbf{x}} \sim N(\mathbf{U}^t(\boldsymbol{\theta})\mathbf{U}(\boldsymbol{\theta}')\mathbf{m}_m, (\sigma^2/L)\mathbf{I}_2)$ and $\mathbf{U}_\perp^t(\boldsymbol{\theta})\overline{\mathbf{x}} \sim N(\mathbf{U}_\perp^t(\boldsymbol{\theta})\mathbf{U}(\boldsymbol{\theta}')\mathbf{m}_m, (\sigma^2/L)\mathbf{I}_{N-2})$. Thus, the density of $(L/\sigma^2)\overline{\mathbf{x}}^t\mathbf{U}(\boldsymbol{\theta})\mathbf{U}^t(\boldsymbol{\theta})\overline{\mathbf{x}}$ is noncentral Chi-squared [12] with noncentrality parameter

$$\delta_m = \frac{L}{\sigma^2}\,\|\mathbf{U}^t(\boldsymbol{\theta})\mathbf{U}(\boldsymbol{\theta}')\mathbf{m}_m\|^2. \tag{37}$$

The density for $(L/\sigma^2)\overline{\mathbf{x}}^t\mathbf{U}_\perp(\boldsymbol{\theta})\mathbf{U}_\perp^t(\boldsymbol{\theta})\overline{\mathbf{x}}$ is independent of $(L/\sigma^2)\overline{\mathbf{x}}^t\mathbf{U}(\boldsymbol{\theta})\mathbf{U}^t(\boldsymbol{\theta})\overline{\mathbf{x}}$ and is also noncentral Chi-squared with noncentrality parameter

$$\delta_{m\perp} = \frac{L}{\sigma^2}\,\|\mathbf{U}_\perp^t(\boldsymbol{\theta})\mathbf{U}(\boldsymbol{\theta}')\mathbf{m}_m\|^2. \tag{38}$$

Hence, the test statistic $((N-2)/2)T_m(\boldsymbol{\theta})$ is doubly noncentral F-distributed [12] with 2 and $N-2$ degrees of freedom and noncentrality parameters δ_m and $\delta_{m\perp}$, respectively. The resulting probability of detection is written as

$$P_{D_m} = \int_{t_m}^{\infty} F_{2,\,N-2}(\delta_m,\,\delta_{m\perp},\,T_m)\,dT_m. \tag{39}$$

The difference between P_{D_m} and P_{FP_m} is the noncentrality parameters δ_m and $\delta_{m\perp}$ resulting from the presence of a source.

We may obtain insight as to the effect of location errors by using (30) to show that the sum of the parameters defined in (37) and (38) is

$$\delta_m + \delta_{m\perp} = \mathrm{SNR}_m \tag{40}$$

where $\mathrm{SNR}_m = L\|\mathbf{m}_m\|^2/\sigma^2$ is the ratio of signal energy to noise power, since $\|\mathbf{m}_m\|^2$ is the energy in the dipole and σ^2/L is the noise variance after averaging. Hence, the noncentrality parameter associated with the numerator of $((N-2)/2)T_m(\boldsymbol{\theta})$ is decreased by a location error, while the noncentrality parameter of the denominator increases. These effects reduce the probability of detecting a source.

If we set $\boldsymbol{\theta} = \boldsymbol{\theta}'$, that is, we are detecting at the true location, then the noncentrality parameters are

$$\delta_m = \mathrm{SNR}_m, \qquad \delta_{m\perp} = 0. \tag{41}$$

In this case the test statistic $((N-2)/2)T_m(\boldsymbol{\theta}')$ is singly noncentral F-distributed with 2 and $N-2$ degrees of freedom and noncentrality parameter $\delta_m = \mathrm{SNR}_m$.

B. Fixed Known Dipole Orientation

Transform the goodness of fit expression (9) according to (28) to obtain the test statistic

$$T_f(\boldsymbol{\theta}) = \frac{\sum_{i=1}^{L}\mathbf{x}^t(i)\mathbf{v}(\boldsymbol{\theta})\mathbf{v}^t(\boldsymbol{\theta})\mathbf{x}(i)}{\sum_{i=1}^{L}\mathbf{x}^t(i)\mathbf{V}_\perp(\boldsymbol{\theta})\mathbf{V}_\perp^t(\boldsymbol{\theta})\mathbf{x}(i)} \underset{\text{no dipole}}{\overset{\text{dipole}}{\gtrless}} \frac{\beta_f}{1-\beta_f} \tag{42}$$

where $\mathbf{V}_\perp(\boldsymbol{\theta})$ is an $N \times (N-1)$ dimensional matrix whose columns are an orthonormal basis for the space orthogonal to $\mathbf{v}(\boldsymbol{\theta})$ and β_f is the goodness of fit test threshold.

When there is no source present we have $\mathbf{x}(i) \sim N(\mathbf{0}, \sigma^2\mathbf{I}_N)$ so $\mathbf{v}^t(\boldsymbol{\theta})\mathbf{x}(i) \sim N(0, \sigma^2)$ and $\mathbf{V}_\perp^t(\boldsymbol{\theta})\mathbf{x}(i) \sim N(\mathbf{0}, \sigma^2\mathbf{I}_{N-1})$. Thus, $T_f(\boldsymbol{\theta})$ is the ratio of independent Chi-squared random variables. The numerator is χ_L^2 and the denominator is $\chi_{L(N-1)}^2$ so $(N-1)T_f(\boldsymbol{\theta}) \sim F_{L,\,L(N-1)}$. The probability of a false positive decision is, therefore, expressed as

$$P_{\mathrm{FP}_f} = \int_{t_f}^{\infty} F_{L,\,L(N-1)}(T_f)\,dT_f \tag{43}$$

where

$$t_f = \left(\frac{\beta_f}{1-\beta_f}\right)(N-1). \tag{44}$$

Note that P_{FP_f} depends only on the threshold and dimensional parameters of the problem.

To compute the probability of detection we assume a true source location at $\boldsymbol{\theta}'$. Thus, $\mathbf{v}^t(\boldsymbol{\theta})\mathbf{x}(i) \sim N(\mathbf{v}^t(\boldsymbol{\theta})\mathbf{v}(\boldsymbol{\theta}')g(i), \sigma^2)$ and $\mathbf{V}_\perp^t(\boldsymbol{\theta})\mathbf{x}(i) \sim N(\mathbf{V}_\perp^t(\boldsymbol{\theta})\mathbf{v}(\boldsymbol{\theta}')g(i), \sigma^2\mathbf{I}_{N-1})$. The probability density function of the test statistic $(N-1)T_f(\boldsymbol{\theta})$ is then $F_{L,\,L(N-1)}(\delta_f, \delta_{f\perp})$ where

$$\delta_f = \frac{1}{\sigma^2}\,(\mathbf{v}^t(\boldsymbol{\theta})\mathbf{v}(\boldsymbol{\theta}'))^2\sum_{i=1}^{L} g^2(i) \tag{45}$$

and

$$\delta_{f\perp} = \frac{1}{\sigma_2} \|\mathbf{V}_\perp^t(\boldsymbol{\theta})\mathbf{v}(\boldsymbol{\theta}')\|^2 \sum_{i=1}^{L} g^2(i). \tag{46}$$

Therefore, the probability of detection for the known dipole orientation model is

$$P_{D_f} = \int_{t_f}^{\infty} F_{L,\,L(N-1)}(\delta_f,\, \delta_{f\perp},\, T_f)\, dT_f. \tag{47}$$

The effect of location errors may be evaluated by studying the noncentrality parameters in (45) and (46). Since, by definition $\mathbf{v}(\boldsymbol{\theta})\mathbf{v}^t(\boldsymbol{\theta}) + \mathbf{V}_\perp(\boldsymbol{\theta})\mathbf{V}_\perp^t(\boldsymbol{\theta}) = \mathbf{I}_N$, we have

$$\mathrm{SNR}_f = \delta_f + \delta_{f\perp} \tag{48}$$

where $\mathrm{SNR}_f = (1/\sigma^2)\sum_{i=1}^{L} g^2(i)$ is the ratio of the energy associated with the dipole to the noise power. Hence, a location error reduces the noncentrality parameter associated with the numerator of $(N-1)T_f(\boldsymbol{\theta})$ and increases the noncentrality parameter in the denominator, producing decreased P_{D_f}. This decrease in P_{D_f} is dependent only on the angle ϕ between the assumed pattern $\mathbf{v}(\boldsymbol{\theta})$ and the actual pattern $\mathbf{v}(\boldsymbol{\theta}')$. Both $\mathbf{v}(\boldsymbol{\theta})$ and $\mathbf{v}(\boldsymbol{\theta}')$ are unit norm vectors so

$$\|\mathbf{v}^t(\boldsymbol{\theta})\mathbf{v}(\boldsymbol{\theta}')\|^2 = \cos^2\phi. \tag{49}$$

This implies that $\delta_f = (\cos^2\phi)\mathrm{SNR}_f$ while $\delta_{f\perp} = (\sin^2\phi)\,\mathrm{SNR}_f$ and, thus, the loss in P_{D_f} increases as the angle between $\mathbf{v}(\boldsymbol{\theta})$ and $\mathbf{v}(\boldsymbol{\theta}')$ increases. Note that since $\mathbf{v}(\boldsymbol{\theta}) = \mathbf{U}(\boldsymbol{\theta})\mathbf{m}_o$, this analysis also applies to errors between the true moment orientation and the one assumed when forming the test statistic. If $\boldsymbol{\theta} = \boldsymbol{\theta}'$, the true moment orientation is $\mathbf{m}_o'$ and the assumed orientation is $\mathbf{m}_o$, then (49) implies $\cos^2(\phi) = \|\mathbf{m}_o^t\mathbf{m}_o'\|^2$.

When $\boldsymbol{\theta} = \boldsymbol{\theta}'$, then

$$\delta_f = \mathrm{SNR}_f, \qquad \delta_{f\perp} = 0. \tag{50}$$

The probability density function of $(N-1)T_f(\boldsymbol{\theta}')$ is then singly noncentral F-distributed, $F_{L,\,L(N-1)}(\mathrm{SNR}_f)$.

C. Fixed Unknown Dipole Orientation

When the dipole orientation $\mathbf{m}_o$ is unknown, we transform (17) using (28) to obtain the test statistic

$$T_u(\boldsymbol{\theta}) = \frac{\sum_{i=1}^{L} \mathbf{x}^t(i)\mathbf{v}(\boldsymbol{\theta})\mathbf{v}^t(\boldsymbol{\theta})\mathbf{x}(i)}{\sum_{i=1}^{L} \mathbf{x}^t(i)\mathbf{V}_\perp(\boldsymbol{\theta})\mathbf{V}_\perp^t(\boldsymbol{\theta})\mathbf{x}(i)} \underset{\text{no dipole}}{\overset{\text{dipole}}{\gtrless}} \frac{\beta_u}{1-\beta_u}. \tag{51}$$

$T_u(\boldsymbol{\theta})$ is identical to $T_f(\boldsymbol{\theta})$ except that here $\mathbf{v}(\boldsymbol{\theta})$ and $\mathbf{V}_\perp(\boldsymbol{\theta})$ are random since they depend on $\hat{\mathbf{m}}_o(\boldsymbol{\theta})$ given in (16).

If we condition $T_u(\boldsymbol{\theta})$ on $\mathbf{v}(\boldsymbol{\theta})$, that is, assume $\mathbf{v}(\boldsymbol{\theta})$ is known, then we remove the effect of $\mathbf{v}(\boldsymbol{\theta})$ being random and see that $f(T_u(\boldsymbol{\theta})|\mathbf{v}(\boldsymbol{\theta})) = f(T_f(\boldsymbol{\theta}))$, because $T_u(\boldsymbol{\theta})$ and $T_f(\boldsymbol{\theta})$ are now identical. Removing the conditioning on $\mathbf{v}(\boldsymbol{\theta})$ to obtain $f(T_u(\boldsymbol{\theta}))$ is difficult in general due to the complexity of the statistics of $\hat{\mathbf{m}}_o(\boldsymbol{\theta})$ given in (16). However, we can infer the performance in several special cases.

Note that $\hat{\mathbf{m}}_o(\boldsymbol{\theta})$ is the eigenvector associated with the largest eigenvalue of the 2×2 sample covariance matrix $(1/L)\sum_{i=1}^{L} \mathbf{z}(i)\mathbf{z}^t(i)$ where $\mathbf{z}(i) = \mathbf{U}^t(\boldsymbol{\theta})\mathbf{x}(i)$. For $L \gg 2$ the sample covariance matrix converges to the true covariance matrix. Under this condition we may approximate $\hat{\mathbf{m}}_o(\boldsymbol{\theta})$ as a fixed known quantity in which case $f(T_u(\boldsymbol{\theta})) \approx f(T_f(\boldsymbol{\theta}))$.

In general (23) implies $T_f(\boldsymbol{\theta}) \le T_u(\boldsymbol{\theta}) \le T_r(\boldsymbol{\theta})$ [for $T_r(\boldsymbol{\theta})$ see (53)], so we conclude that the threshold t_u required to achieve a given P_{FP} will satisfy

$$t_f \le t_u \le t_r \tag{52}$$

where t_r is the threshold for the variable dipole moment orientation test given in (55). For $L \gg 2$, we expect $t_u \approx t_f$, and $P_{D_u} \approx P_{D_f}$.

D. Variable Dipole Moment Orientation

Transform the goodness of fit expression (21) according to (28) to obtain the test statistic

$$T_r(\boldsymbol{\theta}) = \frac{\sum_{i=1}^{L} \mathbf{x}^t(i)\mathbf{U}(\boldsymbol{\theta})\mathbf{U}^t(\boldsymbol{\theta})\mathbf{x}(i)}{\sum_{i=1}^{L} \mathbf{x}^t(i)\mathbf{U}_\perp(\boldsymbol{\theta})\mathbf{U}_\perp^t(\boldsymbol{\theta})\mathbf{x}(i)} \underset{\text{nodipole}}{\overset{\text{dipole}}{\gtrless}} \frac{\beta_r}{1-\beta_r} \tag{53}$$

where $\mathbf{U}_\perp(\boldsymbol{\theta})$ is defined as in Section III-A. If no source is present, $\mathbf{U}^t(\boldsymbol{\theta})\mathbf{x}(i) \sim N(\mathbf{0},\, \sigma^2\mathbf{I}_2)$ and $\mathbf{U}_\perp^t(\boldsymbol{\theta})\mathbf{x}(i) \sim N(\mathbf{0},\, \sigma^2\mathbf{I}_{N-2})$. Thus, $((N-2)/2)T_r(\boldsymbol{\theta}) \sim F_{2L,\,(N-2)L}$ and

$$P_{\mathrm{FP}_r} = \int_{t_r}^{\infty} F_{2L,\,(N-2)L}(T_r)\, dT_r \tag{54}$$

where

$$t_r = \left(\frac{\beta_r}{1-\beta_r}\right)\left(\frac{N-2}{2}\right). \tag{55}$$

To compute the probability of detection we assume a true source location $\boldsymbol{\theta}'$. Thus, $\mathbf{U}^t(\boldsymbol{\theta})\mathbf{x}(i) \sim N(\mathbf{U}^t(\boldsymbol{\theta})\mathbf{U}(\boldsymbol{\theta}')\mathbf{m}(i),\, \sigma^2\mathbf{I}_2)$, and $\mathbf{U}_\perp^t(\boldsymbol{\theta})\mathbf{x}(i) \sim N(\mathbf{U}_\perp^t(\boldsymbol{\theta})\mathbf{U}(\boldsymbol{\theta}')\mathbf{m}(i),\, \sigma^2\mathbf{I}_{N-2})$. This implies $((N-2)/2)T_r(\boldsymbol{\theta}) \sim F_{2L,\,(N-2)L}(\delta_r,\, \delta_{r\perp})$ where the noncentrality parameters are

$$\delta_r = \frac{1}{\sigma^2}\sum_{i=1}^{L} \|\mathbf{U}^t(\boldsymbol{\theta})\mathbf{U}(\boldsymbol{\theta}')\mathbf{m}(i)\|^2 \tag{56}$$

and

$$\delta_{r\perp} = \frac{1}{\sigma^2}\sum_{i=1}^{L} \|\mathbf{U}_\perp^t(\boldsymbol{\theta})\mathbf{U}(\boldsymbol{\theta}')\mathbf{m}(i)\|^2 \tag{57}$$

so

$$P_{D_r} = \int_{t_r}^{\infty} F_{2L,\,(N-2)L}(\delta_r,\, \delta_{r\perp},\, T_r)\, dT_r. \tag{58}$$

As in the previous cases, we may write

$$\mathrm{SNR}_r = \delta_r + \delta_{r\perp} \tag{59}$$

where $\mathrm{SNR}_r = (1/\sigma^2)\sum_{i=1}^{L} \|\mathbf{m}(i)\|^2$ is the ratio of the signal energy associated with the dipole to the noise power. The effect of a location error is to decrease the numerator noncentrality parameter and increase the denominator noncentrality parameter in $T_r(\boldsymbol{\theta})$, which results in decreased probability of detection.

When $\boldsymbol{\theta} = \boldsymbol{\theta}'$, then $\delta_r = \mathrm{SNR}_r$ and $\delta_{r\perp} = 0$.

E. The Effect of Model Mismatch

The statistical analysis given in the preceding subsections provides a mechanism for addressing the effect of choosing the wrong model. Thus, the analysis indicates the benefit of explicitly including variable amplitude or orientation in the test when it is actually present, and conversely, the potential performance loss associated with assuming a more general model than the true one. In the discussion below we assume the location is known, so $\boldsymbol{\theta} = \boldsymbol{\theta}'$.

1) Overmodeling: Consider assuming a variance based model when the data is actually described by a fixed dipole with constant amplitude. In this case, $\mathbf{m}(i) = \mathbf{m}_o g$ and, therefore

$$\mathrm{SNR}_r = \mathrm{SNR}_f = \mathrm{SNR}_m = L\,\frac{g^2}{\sigma^2}. \tag{60}$$

Hence, the noncentrality parameter is identical for these three models and the effect of model mismatch is captured entirely by the differing degrees of freedom associated with the F distributions for each test. In general, the P_D will be highest for the test statistic with the fewest degrees of freedom, assuming a fixed P_{FP}.

The effect of assuming a variable dipole orientation when the data actually has a fixed orientation but variable amplitude is also captured entirely by the increased degrees of freedom associated with $T_r(\boldsymbol{\theta})$ relative to $T_f(\boldsymbol{\theta})$ since for $\mathbf{m}(i) = \mathbf{m}_o g(i)$ we have that $\mathrm{SNR}_f = \mathrm{SNR}_r$, that is, the noncentrality parameters are identical.

2) Undermodeling: If the model is underspecified, then both the degrees of freedom and noncentrality parameters are affected. First, suppose the dipole has fixed orientation but variable amplitude. The noncentrality parameter for the mean-based test is

$$\mathrm{SNR}_m = L\,\frac{\|\mathbf{m}_m\|^2}{\sigma^2} \tag{61}$$

$$= \frac{L}{\sigma^2}\,\mu_g^2 \tag{62}$$

where $\mu_g = (1/L)\sum_{i=1}^{L} g(i)$ is the mean of the dipole moment amplitude across trials. Similarly,

$$\mathrm{SNR}_f = \mathrm{SNR}_r = \frac{L}{\sigma^2}\left(\frac{1}{L}\sum_{i=1}^{L} g^2(i)\right) \tag{63}$$

$$= \frac{L}{\sigma^2}\,\xi_g^2 \tag{64}$$

where ξ_g^2 is the second moment (statistical sense) of the dipole moment amplitude across trials. Since the second moment is the sum of the squared mean and variance, $\xi_g^2 = \mu_g^2 + \sigma_g^2$, where $\sigma_g^2 = (1/L)\sum_{i=1}^{L}(g(i) - \mu_g)^2$ we see from (62) and (64) that

$$\mathrm{SNR}_f = \mathrm{SNR}_m + L(\sigma_g^2/\sigma^2). \tag{65}$$

Note that $L(\sigma_g^2/\sigma^2)$ is nonnegative, so $\mathrm{SNR}_m \leq \mathrm{SNR}_f$ with equality when $\sigma_g^2 = 0$. Thus, the noncentrality parameter for the variance-based tests is lower bounded by that of the mean-based test.

An upper bound on the variance-based noncentrality parameter is obtained by considering the ratio

$$\frac{\mathrm{SNR}_f}{\mathrm{SNR}_m} = \frac{\xi_g^2}{\mu_g^2} \tag{66}$$

$$= L\,\frac{\sum_{i=1}^{L} g^2(i)}{\left(\sum_{i=1}^{L} g(i)\right)^2}. \tag{67}$$

The data under study is assumed to result from multiple independent trials or observations of the same underlying biological structure and event. Hence, we may assume that the likelihood of current flow inversion is negligible and, therefore, all the $g(i)$ have the same sign, that is, $g(i) \geq 0$ or $g(i) \leq 0$ for all i. This implies that

$$\frac{\sum_{i=1}^{L} g^2(i)}{\left(\sum_{i=1}^{L} g(i)\right)^2} \leq 1 \tag{68}$$

and, thus, $\mathrm{SNR}_f \leq L(\mathrm{SNR}_m)$. One example where equality can be reached is when $g(1) = \alpha$ and $g(i) = 0$ for all $i \neq 1$.

Equations (65)–(68) imply the bounds on SNR_f are expressed in terms of SNR_m as

$$\mathrm{SNR}_m \leq \mathrm{SNR}_f \leq L(\mathrm{SNR}_m). \tag{69}$$

For data in which there is very little variance we expect SNR_f to be near the lower bound. Data in which the moment amplitudes are drawn from a heavy-tailed distribution are likely to be near the upper bound since a heavy-tailed distribution is likely to generate one relatively large $g(i)$. Note that if current flow inversion is possible, then the upper bound of (69) is eliminated since it is then possible for $\mathrm{SNR}_m = 0$ while $\mathrm{SNR}_f > 0$.

Lastly, suppose the data contains a variable dipole orientation, and we employ the fixed orientation test $T_f(\boldsymbol{\theta})$. It is straightforward to show that $(N-1)T_f(\boldsymbol{\theta})$ has noncentrality parameter $\mathrm{SNR}_f = (1/\sigma^2)\sum_{i=1}^{L} \|\mathbf{m}_o^t \mathbf{m}(i)\|^2$. Clearly, $\mathrm{SNR}_f \leq \mathrm{SNR}_r$ with the difference dependent on how much $\mathbf{m}(i)$ rotates. If the difference is small, then $T_f(\boldsymbol{\theta})$ may give better performance because it has fewer degrees of freedom.

F. Localization

Least squares dipole fitting may be used to localize a dipolar source by finding the location $\boldsymbol{\theta}$ that maximizes the appropriate test statistic $T(\boldsymbol{\theta})$. Complete characterization of localization performance is difficult since $T(\boldsymbol{\theta})$ is a random surface and the joint probability density function of $T(\boldsymbol{\theta})$ over all locations $\boldsymbol{\theta}$ may be impossible to obtain. However, the mean of the random surface $T(\boldsymbol{\theta})$ for each dipole moment is easily obtained by numerically integrating the probability density functions determined in Sections III-A–D.

As a second metric of localization performance we consider the probability that $T(\boldsymbol{\theta}') < T(\boldsymbol{\theta})$ where $\boldsymbol{\theta}'$ is the true location and $\boldsymbol{\theta}$ is any other location. This is the probability that the source will be incorrectly localized at $\boldsymbol{\theta}$ rather than at the true location

$\boldsymbol{\theta}'$. Beginning with the constant dipole case, we note that the condition $T_m(\boldsymbol{\theta}') < T_m(\boldsymbol{\theta})$ is equivalent to

$$\overline{\mathbf{x}}^t\mathbf{U}(\boldsymbol{\theta})\mathbf{U}^t(\boldsymbol{\theta})\overline{\mathbf{x}} - \overline{\mathbf{x}}^t\mathbf{U}(\boldsymbol{\theta}')\mathbf{U}^t(\boldsymbol{\theta}')\overline{\mathbf{x}} > 0 \tag{70}$$

a result which is a consequence of (30). Rewrite (70) as the quadratic form $\overline{\mathbf{x}}^t\mathbf{A}\overline{\mathbf{x}} > 0$, where

$$\mathbf{A} = [\mathbf{U}(\boldsymbol{\theta})\mathbf{U}(\boldsymbol{\theta}')]\begin{bmatrix}\mathbf{I}_2 & \mathbf{0}\\ \mathbf{0} & -\mathbf{I}_2\end{bmatrix}\begin{bmatrix}\mathbf{U}^t(\boldsymbol{\theta})\\ \mathbf{U}^t(\boldsymbol{\theta}')\end{bmatrix}. \tag{71}$$

The matrix $\mathbf{A}$ is symmetric and, thus, has eigendecomposition $\mathbf{A} = \mathbf{Q}\boldsymbol{\Delta}\mathbf{Q}^t$ where $\mathbf{Q}$ is an orthonormal matrix with columns $\mathbf{q}(i)$ and $\boldsymbol{\Delta} = \mathrm{diag}\{\lambda_1, \lambda_2, \lambda_3, \lambda_4\}$. Note that (71) implies that in general $\mathbf{A}$ has both positive and negative eigenvalues. Assume for purposes of illustration that $\lambda_1, \lambda_2 > 0$ and $\lambda_3, \lambda_4 < 0$. In this case, (70) is rewritten as

$$\sum_{i=1}^{2}|\lambda_i|\,|\overline{\mathbf{x}}^t\mathbf{q}(i)|^2 > \sum_{i=3}^{4}|\lambda_i|\,|\overline{\mathbf{x}}^t\mathbf{q}(i)|^2. \tag{72}$$

Since the $\mathbf{q}(i)$ are orthonormal, $|\overline{\mathbf{x}}^t\mathbf{q}(i)|^2$ is distributed as $\chi^2_N(\delta_i)$ and is independent of $|\overline{\mathbf{x}}^t\mathbf{q}(j)|^2$ for $j \neq i$, where the noncentrality parameter is $\delta_i = (L/\sigma^2)\|\mathbf{m}_m^t\mathbf{U}^t(\boldsymbol{\theta}')\mathbf{q}(i)\|^2$. Thus, the random variable on the left-hand side of (72), denoted as C_1, is $\chi^2_{2N}(|\lambda_1|\delta_1 + |\lambda_2|\delta_2)$ while the right-hand side of (72), denoted as C_2 is distributed as $\chi^2_{2N}(|\lambda_3|\delta_3 + |\lambda_4|\delta_4)$. Also, C_1 and C_2 are statistically independent. Thus, the probability that $C_1 > C_2$ may be written in terms of their respective densities as

$$P_m(\boldsymbol{\theta}) = \int_0^\infty \left[\int_{c_2}^\infty f_{C_1}(c_1)\,dc_1\right] f_{C_2}(c_2)\,dc_2. \tag{73}$$

Similar approaches may be used to derive the probability that $T_f(\boldsymbol{\theta}') < T_f(\boldsymbol{\theta})$ or $T_r(\boldsymbol{\theta}') < T_r(\boldsymbol{\theta})$. The condition $T_f(\boldsymbol{\theta}') < T_f(\boldsymbol{\theta})$ is equivalent to

$$\sum_{i=1}^{L}\mathbf{x}^t(i)\mathbf{A}\mathbf{x}(i) > 0 \tag{74}$$

where $\mathbf{A} = \mathbf{v}(\boldsymbol{\theta})\mathbf{v}^t(\boldsymbol{\theta}) - \mathbf{v}(\boldsymbol{\theta}')\mathbf{v}^t(\boldsymbol{\theta}')$. In this case $\mathbf{A}$ has two nonzero eigenvalues, $\lambda_1 > 0$ and $\lambda_2 < 0$, with corresponding eigenvectors $\mathbf{q}_1$ and $\mathbf{q}_2$. The condition (74) may be shown to be equivalent to $C_1 > C_2$ where $C_1 \sim \chi^2_{LN}(\delta_1)$, $C_2 \sim \chi^2_{LN}(\delta_2)$, and $\delta_k = (|\lambda_k|^2\mathbf{q}_k^t\mathbf{v}(\boldsymbol{\theta}'))^2(\sum_{i=1}^{L} g^2(i))/\sigma^2$, $k = 1, 2$. Thus, the probability that (74) is true may be computed using the appropriate densities in (73).

Finally, the condition $T_r(\boldsymbol{\theta}') < T_r(\boldsymbol{\theta})$ may be written as in (74) where $\mathbf{A}$ is given by (71). The expression for the probability that $T_r(\boldsymbol{\theta}') < T_r(\boldsymbol{\theta})$ is then derived in terms of the eigenvectors and eigenvalues of $\mathbf{A}$ analogously to the constant dipole case.

IV. Results

A. Model Performance Comparison

The relative performance of the dipole detection schemes is illustrated by computing the probability of detection at the true source location $\boldsymbol{\theta}'$ as a function of the noncentrality parameters assuming equal P_{FP}. We consider two cases: $P_{\mathrm{FP}} = 10^{-12}$ and $P_{\mathrm{FP}} = 10^{-3}$. The corresponding goodness of fit thresholds for the constant dipole model are $\beta_m = 0.79$ and $\beta_m = 0.33$, respectively. Under the assumption of spatially white noise, use

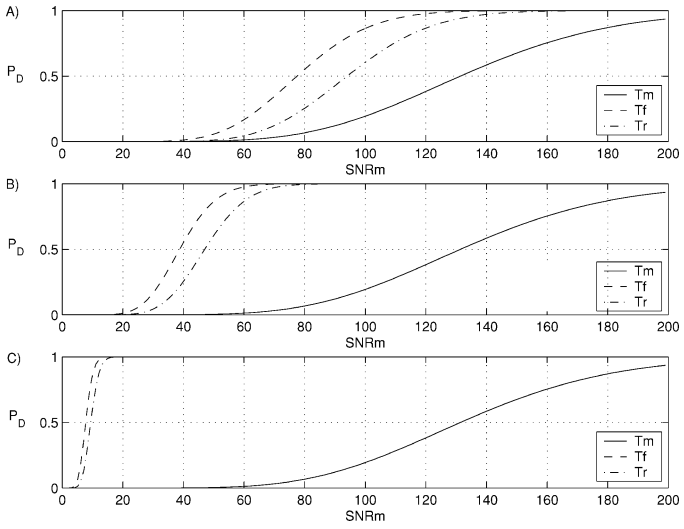

Fig. 1. Probability of detecting a dipolar source at the true location as a function of SNR_m with a probability of false positive of $P_{\mathrm{FP}} = 10^{-12}$ (constant dipole detection test goodness of fit threshold $\beta_m = 0.79$). (A) Zero source variance, $\mathrm{SNR}_r = \mathrm{SNR}_f = \mathrm{SNR}_m$. (B) Modest source variance, $\mathrm{SNR}_r = \mathrm{SNR}_f = 2\mathrm{SNR}_m$. (C) Maximum source variance, $\mathrm{SNR}_r = \mathrm{SNR}_f = 10\mathrm{SNR}_m$.

of larger thresholds , such as $\beta_m = 0.95$, is not warranted as it penalizes the probability of detection without providing practically useful gains in P_{FP}.

We use $N = 37$ sensors in the configuration employed by the Magnes II Biomagnetometer, a spherical shell head model with a 13 cm radius, and $L = 10$ data samples. Selecting the range $0.1 \leq \mathrm{SNR}_m \leq 200$, we compute the probability of detection for three cases: 1) zero source variance $\mathrm{SNR}_r = \mathrm{SNR}_f = \mathrm{SNR}_m$, 2) modest source variance $\mathrm{SNR}_r = \mathrm{SNR}_f = 2\mathrm{SNR}_m$, and 3) maximum source variance $\mathrm{SNR}_r = \mathrm{SNR}_f = L(\mathrm{SNR}_m)$. The corresponding probabilities of detection are shown in Figs. 1 and 2.

As the noncentrality parameter increases, the probability of detection for all cases tends to one. This is reasonable since the noncentrality parameter represents the signal to noise ratio. Similarly, as the probability of a false positive decision increases, the probability of detection also increases for a fixed value of SNR_m. Conversely, as the goodness of fit threshold β increases, the probability of detection decreases for a given SNR. Note from Fig. 2(A) that when $P_{\mathrm{FP}} = 10^{-3}$ a P_{D_f} of 0.9 is obtained for $\mathrm{SNR}_m \approx 30$. To obtain $P_{D_f} = 0.9$ when $P_{\mathrm{FP}} = 10^{-12}$ (see Fig. 1), we require $\mathrm{SNR}_m \approx 200$, a factor of almost seven larger. The constant moment test T_m generally performs relatively poor at the very small P_{FP} corresponding to large goodness of fit thresholds, as shown Fig. 1.

Figs. 1 and 2 may be used to illustrate the effects of using the wrong model by comparing P_D for the different tests. Panel (A) of both figures illustrates the effect of overmodeling since in this case (60) holds, that is, the SNR is identical for each model. As shown in Fig. 1(A), there is a penalty in detection performance for overmodeling by using either T_f or T_r at $P_{\mathrm{FP}} = 10^{-3}$. The penalty associated with assuming a variable dipole orientation when the orientation is actually fixed and known is illustrated in all six cases by comparing P_{D_f} to P_{D_r}. We see that $P_{D_f} > P_{D_r}$ in every case. The effects of undermodeling is also evident in

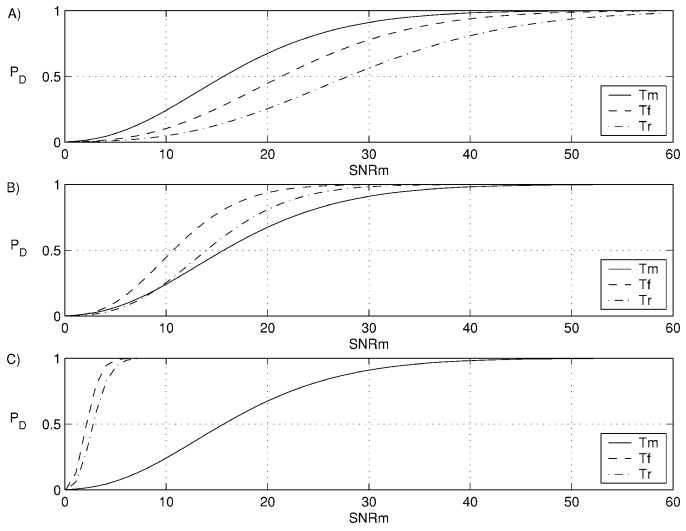

Fig. 2. Probability of detecting a dipolar source at the true location as a function of SNR_m with $P_{\mathrm{FP}} = 10^{-3}$ (constant dipole model detection test goodness of fit threshold $\beta_m = 0.33$). (A) Zero source variance, $\mathrm{SNR}_r = \mathrm{SNR}_f = \mathrm{SNR}_m$. (B) Modest source variance, $\mathrm{SNR}_r = \mathrm{SNR}_f = 2\mathrm{SNR}_m$. (C) Maximum source variance, $\mathrm{SNR}_r = \mathrm{SNR}_f = 10\mathrm{SNR}_m$.

Figs. 1 and 2, although the degree of performance loss now depends on the relative values of the SNR. For example, panel (B) of both figures compares P_{D_m} to P_{D_f} and P_{D_r} assuming the SNR of the two variance based models are twice that of the constant moment model, while panel (C) depicts performance assuming a factor of ten differential. There is a substantial penalty for using a constant dipole model even when the true dipole has modest variance.

B. Effect of Location Errors

The effect of using the wrong location when detecting the presence of a source is illustrated by assuming the true source location $\boldsymbol{\theta}'$ is placed 2.5 cm directly under the center of the sensor array. We then compute $P_{D_m}, P_{D_f}, P_{D_r}$ for neighboring values $\boldsymbol{\theta}$ having the same radius as the true source as shown in Fig. 3. The results in Fig. 3 are obtained by numerically approximating the doubly noncentral F distribution using the methods in [13]. The SNR is chosen so that the probability of detection at the true source location exceeds 0.99 for each model. The probability of detection decreases as $\boldsymbol{\theta}$ moves away from $\boldsymbol{\theta}'$, although not uniformly because the interaction between $\mathbf{U}(\boldsymbol{\theta})$ and $\mathbf{U}(\boldsymbol{\theta}')$ is not solely a function of $||\boldsymbol{\theta} - \boldsymbol{\theta}'||$.

Fig. 4 depicts P_{D_f} as a function of the mismatch angle ϕ defined in (49) assuming $\mathrm{SNR}_f = 140$ and $P_{\mathrm{FP}} = 10^{-12}$. In the vicinity of $\phi = 0$ there is very little loss due to mismatch between $\mathbf{v}(\boldsymbol{\theta})$ and $\mathbf{v}(\boldsymbol{\theta}')$, but the performance degrades rapidly as ϕ increases past 0.4 radians. Note that if $\boldsymbol{\theta} = \boldsymbol{\theta}'$, then Fig. 4 depicts the loss due to errors between the true $\mathbf{m}_o'$ and assumed $\mathbf{m}_o$ moment orientations since then $\cos^2\phi = |\mathbf{m}_o^t \mathbf{m}_o'|^2$.

C. Simulated Detection Performance

Detection performance is simulated using a series of synthetic spikes in noise. The source is located directly under the center of the sensor array 2.5 cm deep and has a fixed moment. One thousand sets of ten spikes are used to empirically estimate the

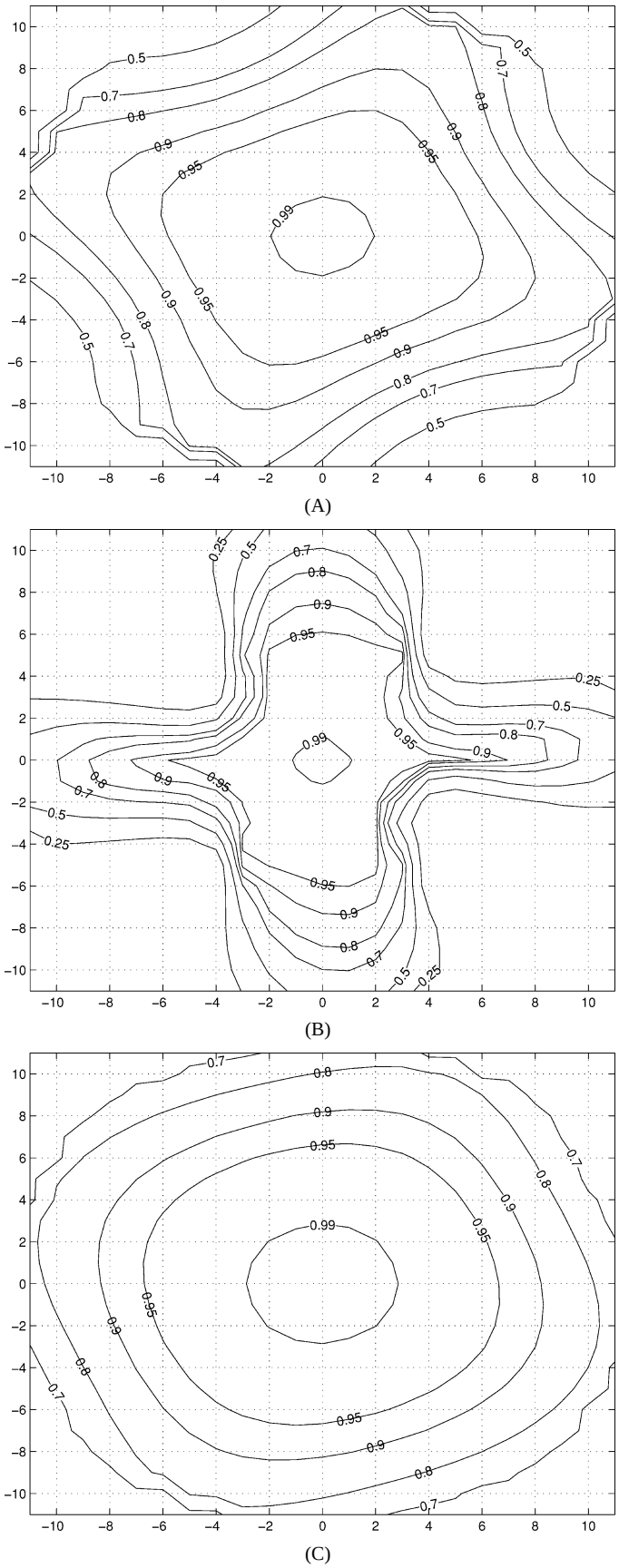

Fig. 3. Contours of constant P_D as a function of assumed source location for $P_{\mathrm{FP}} = 10^{-3}$. The true source location is $(0, 0)$ and the labels on the axes represent location relative to $(0, 0)$ measured in mm. (A) Constant dipole model with $\mathrm{SNR}_m = 45$. (B) Known dipole orientation model with $\mathrm{SNR}_f = 52$. (C) Variable dipole orientation model with $\mathrm{SNR}_r = 67$.

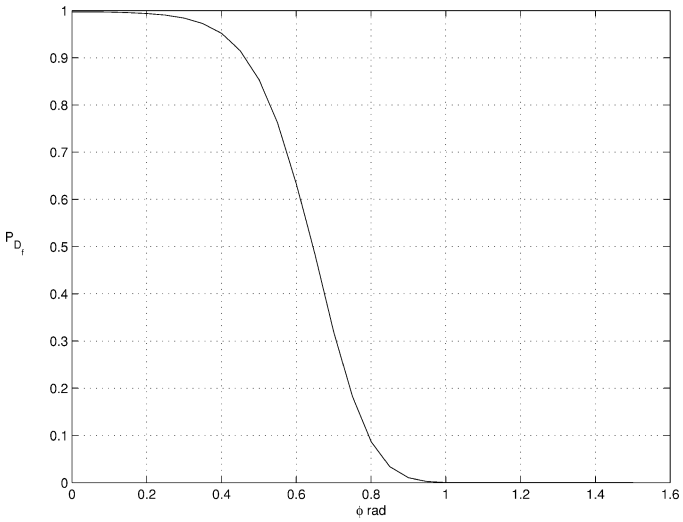

Fig. 4. Probability of detection of the fixed orientation dipole model T_f as a function of the error angle ϕ due to mismatch in location or moment assuming $\mathrm{SNR}_f = 140$ and $P_{\mathrm{FP}} = 10^{-12}$.

probability of detecting the source at the true location as a function of SNR. The dipole moment magnitude $g(i)$ is simulated as $g(i) = a\alpha(i) + b$ where $\alpha(i) \sim \chi^2_2$ and the scaling parameters a and b are chosen so the sample mean and second moment are constant for each set of ten spikes. We assume the scenario represented by Fig. 1(B), that is, $P_{FA} = 10^{-12}$ and $\mathrm{SNR}_r = \mathrm{SNR}_f = \mathrm{SNR}_u = 2(\mathrm{SNR}_m)$. The results shown in Table I agree very well with the expected detection performance depicted in Fig. 1(B). The threshold for T_u is set equal to that used for T_f, since in this experiment $L = 10$ is much greater than two and we expect the estimated moment to be very stable. The detection performance of T_u and T_f is quite similar. Since (23) implies that $T_u \geq T_f$, then we expect $P_{D_u} \geq P_{D_f}$ when the thresholds are identical.

D. Localization of a Dipolar Source

Fig. 5 depicts the mean of $T_m(\boldsymbol{\theta})$, $T_f(\boldsymbol{\theta})$, and $T_r(\boldsymbol{\theta})$ for several SNR's as a function of location $\boldsymbol{\theta}$. We assume the true source location $\boldsymbol{\theta}'$ is directly under the center of the array and display the mean for neighboring locations $\boldsymbol{\theta}$ at the same depth. The maximum in each case is at the true source location, which suggests that if the variability in $T(\boldsymbol{\theta})$ is small, then the source will be correctly localized. Insight regarding the variability in $T(\boldsymbol{\theta})$ is obtained by considering the probability that $T(\boldsymbol{\theta}) > T(\boldsymbol{\theta}')$ as shown in Fig. 6 for the same cases. This figure illustrates the probability that an erroneous location $\boldsymbol{\theta}$ will have a larger goodness of fit than the correct location. As expected, this probability decreases as SNR increases and as the distance between $\boldsymbol{\theta}$ and $\boldsymbol{\theta}'$ increases.

We empirically estimated localization accuracy by calculating the root mean squared error (RMSE) between estimated and true dipole locations using 100 sets of ten synthetic spikes generated as described in Section IV-C. Thus, the RMSE is

$$\mathrm{RMSE} = \left(\frac{1}{100} \sum_{j=1}^{100} \|\hat{\boldsymbol{\theta}}(j) - \boldsymbol{\theta}'\|^2 \right) \tag{75}$$

TABLE I
PERCENTAGE OF CORRECT DETECTION AT THE TRUE DIPOLE LOCATION ASSUMING $\mathrm{SNR}_r = \mathrm{SNR}_u = \mathrm{SNR}_f = 2(\mathrm{SNR}_m)$ AND $P_{FA} = 10^{-12}$ AS A FUNCTION OF TEST STATISTIC T

SNR_m	$T_m(\%)$	$T_f(\%)$	$T_u(\%)$	$T_r(\%)$
25	0	5.5	6.48	0.9
50	0.8	80.2	82.2	52.3
100	19.2	100	100	100
200	94.9	100	100	100

where $\hat{\boldsymbol{\theta}}(j)$ is the estimated location for the jth set of ten spikes. The RMSE is given in Table II for $\mathrm{SNR}_m = 25$ and 50, and $\mathrm{SNR}_r = \mathrm{SNR}_u = \mathrm{SNR}_f = 4(\mathrm{SNR}_m)$. As expected, we see that T_f and T_u give similar performance. Also, substantial improvement is obtained using the models that incorporate signal related variance.

E. Epileptic Spike Localization

The last example employs real data obtained using the Magnes II Biomagnetometer. A total of 18 epileptic spikes were collected from a subject with a left frontal brain lesion. The spatial extent of the lesion precluded *a priori* determination of the exact origin of the spike activity. Localization is performed using only four spikes at a time. Source location estimates are obtained for each possible combination of four spikes out of the 18 available spikes, yielding a total of 3060 trials. The spread of the resulting cluster of estimates is calculated as the average Euclidean distance from each estimate to the cluster center. The cluster spread, also known as the first moment about the center, is a measure of the consistency of the location estimates. The cluster spread and mean location is shown in Table III. The cluster centers are within one centimeter for all four algorithms and consistent with the left frontal location of the lesion. The cluster spread for the variance-based algorithms is significantly less that that for the mean-based algorithm, which suggests that the variance-based algorithms are exploiting the inherent variability in the spike amplitudes to obtain more consistent localization estimates. Note that the true moment orientation is unknown so we do not present results for $T_f(\boldsymbol{\theta})$.

V. SUMMARY

The statistical analysis presented here is used to assess the performance of dipole fitting based detection and localization algorithms for four different models of signal behavior across independent observations of a phenomenon: 1) constant dipole moment, 2) fixed, known moment orientation and variable amplitude, 3) fixed, unknown moment orientation and variable amplitude, and 4) variable moment orientation and amplitude. The last three models provide a mechanism for exploiting variance in the signal with relatively small numbers of data samples. The analysis provides guidelines for choosing the goodness of fit threshold required to obtain a specified probability of incorrectly declaring a dipolar source present in the data. Expressions for the probability of correctly deciding a dipolar source is present are used to compare the various dipole models and assess the impact of using the incorrect model. Localization performance is assessed from the mean value of the detection

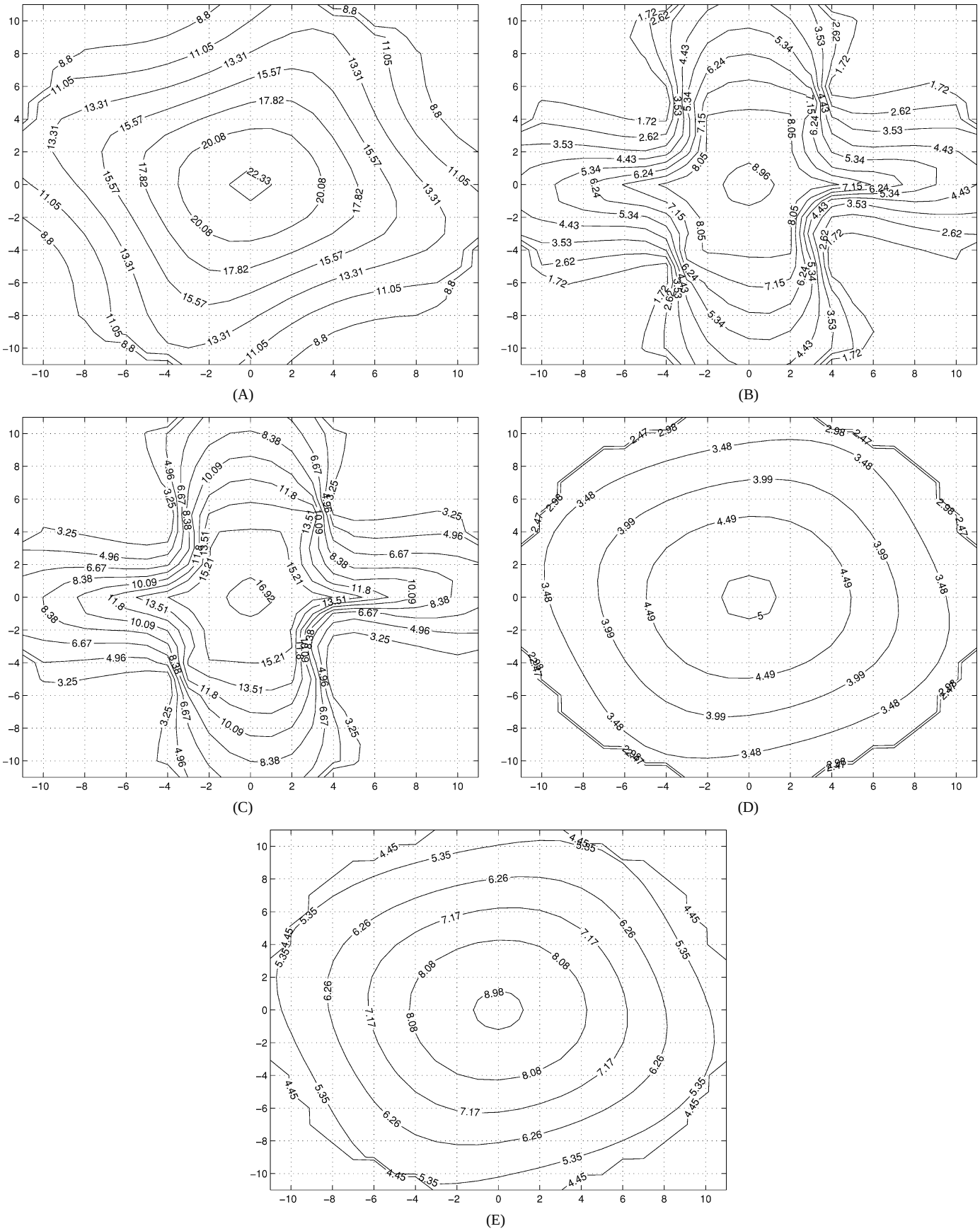

Fig. 5. Expected value of the test statistic T as a function of location. The true source location is at $(0,\ 0)$ and the labels on the axes represent location relative to $(0,\ 0)$ measured in mm. The contours are set at 99%, 89%, 79%, etc. of the maximum value. (A) $E\{T_m\}$ with $\mathrm{SNR}_m = 40$, (B) $E\{T_f\}$ with $\mathrm{SNR}_f = 80$, (C) $E\{T_f\}$ with $\mathrm{SNR}_f = 160$, (D) $E\{T_r\}$ with $\mathrm{SNR}_r = 80$, (E) $E\{T_r\}$ with $\mathrm{SNR}_r = 160$.

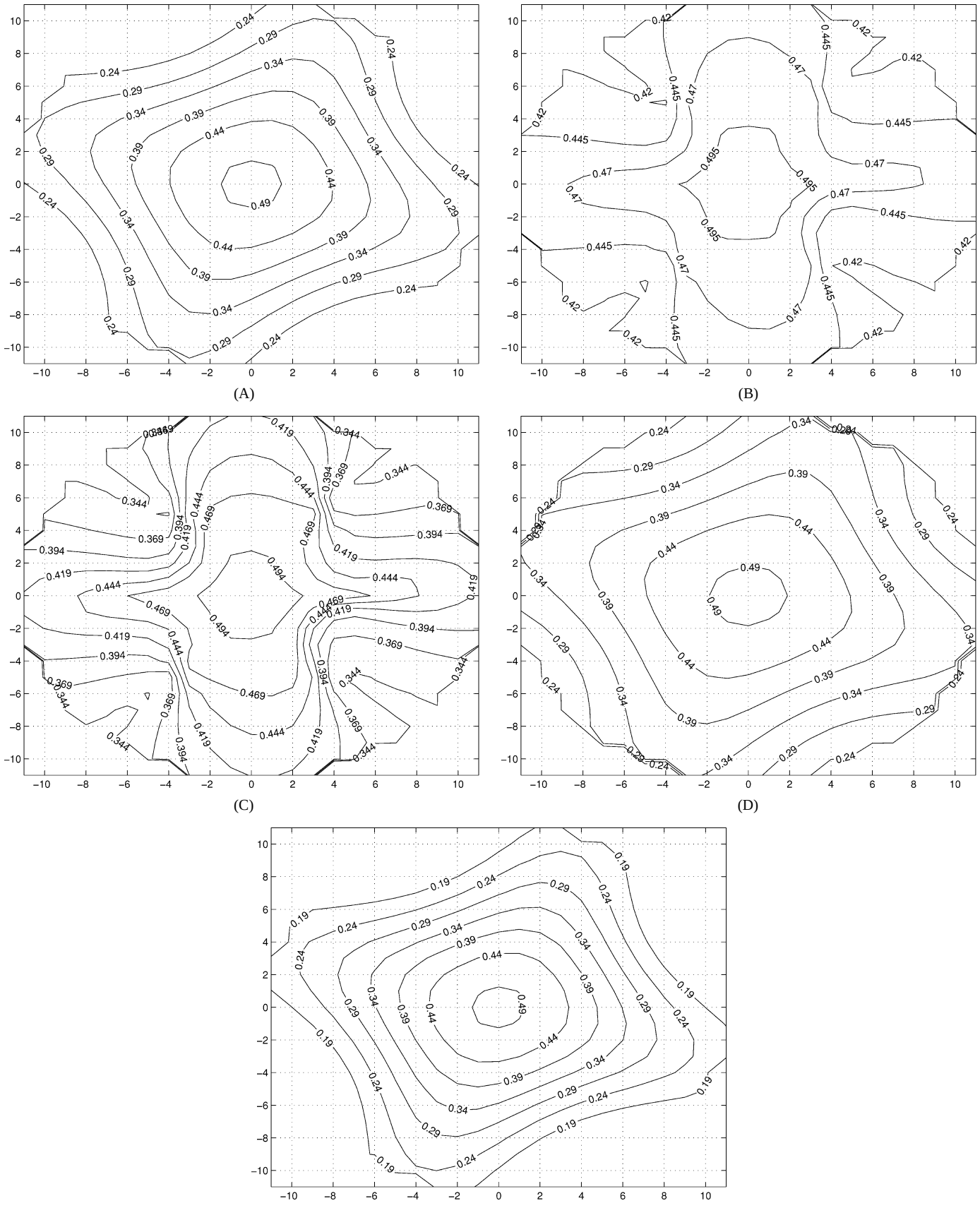

Fig. 6. Probability that $T(\boldsymbol{\theta}) > T(\boldsymbol{\theta}')$ as a function of location. The true source location is $(0, 0)$ and the labels on the axes represent location relative to $(0, 0)$ measured in mm. (A) Constant dipole model with $\mathrm{SNR}_m = 40$. (B) Known dipole orientation model with $\mathrm{SNR}_f = 80$. (C) Known dipole orientation model with $\mathrm{SNR}_f = 160$. (D) Variable dipole orientation model with $\mathrm{SNR}_r = 80$. (E) Variable dipole orientation model with $\mathrm{SNR}_r = 160$.

TABLE II
SYNTHETIC DATA RMS LOCALIZATION ERROR PERFORMANCE FOR $\mathrm{SNR}_f = 4\,\mathrm{SNR}_m$

SNR_m	T_m	T_f	T_u	T_r
25	2.04 cm	0.91 cm	0.90 cm	0.96 cm
50	0.83 cm	0.42 cm	0.39 cm	0.38 cm

TABLE III
THE MEAN CLUSTER LOCATION AND SPREAD FOR LOCALIZATION ESTIMATES OF EPILEPTIC SPIKE DATA

Alg. Type	*Cluster Mean Location*	*Cluster Spread*
T_m	(8.87, 1.3, -4.66) cm	1.80 cm
T_u	(8.5, 1.45, -4.94) cm	1.14 cm
T_r	(8.25, 1.31, -5.10) cm	1.45 cm

statistic as a function of location and by considering the probability that any given location will be incorrectly identified as the true source location. The simulated and measured data experiments verify the analysis and indicate that there is substantial potential benefit associated for explicitly incorporating signal related variance into the dipolar source model.

ACKNOWLEDGMENT

The authors thank Dr. E. Ongossanusi for his insightful comments on several mathematical issues and M. M. Maier for helping in the selection and collection of epileptic spikes. Software for approximating a doubly noncentral F distribution was generously provided by Dr. M. Paolella and Dr. R. Butler.

REFERENCES

[1] J. C. Mosher, P. S. Lewis, and R. M. Leahy, "Multiple dipole modeling and localization ofrom spatio–temporal MEG data," *IEEE Trans. Biomed. Eng.*, vol. 39, pp. 541–557, June 1992.

[2] S. Baillet, J. C. Mosher, and R. M. Leahy, "Electromagnetic brain mapping," *IEEE Signal Processing Mag.*, pp. 14–30, Nov. 2001.

[3] E. Rodriguez, N. George, J. P. Lachaux, J. Martineire, B. Renault, and F. J. Varela, "Perception'shadow: Long-distance synchronization of human brain activity," *Nature*, vol. 397, pp. 430–433, Feb. 1999.

[4] B. D. Van Veen, W. van Drongelen, M. Yuchtman, and A. Suzuki, "Localization of brain electrical activity via linearly constrained minimum variance spatial filtering," *IEEE Trans. Biomed. Eng.*, vol. 44, pp. 867–880, Sept. 1997.

[5] A. M. Dale and M. I. Sereno, "Improved localization of cortical activity by combining EEG and MEG with MRI cortical surface reconstruction: A linear approach," *J. Cogn. Neurosci.*, vol. 5, no. 2, pp. 162–176, 1993.

[6] I. S. Reed, J. D. Mallett, and L. E. Brennan, "Rapid convergence rate in adaptive arrays," *IEEE Trans. Aerosp. Electron. Syst.*, vol. AES-10, pp. 853–863, Nov. 1974.

[7] T.-P. Jung, S. Makeig, M. Westerfield, J. Townsend, E. Courchesne, and T. J. Sejnowski, "Analysis and visualization of single-trial event-related potentials," *Human Brain Mapping*, vol. 14, pp. 166–185, Nov 2001.

[8] ——, "Analyzing and visualizing single-trial event-related potentials," *Adv. Neural Inform. Process. Syst.*, vol. 11, 1999.

[9] P. L. Nunez, *Neocortical Dynamics and Human EEG Rhythms*. Oxford, U.K.: Oxford Univ. Press, 1995.

[10] R. J. Muirhead, *Aspects of Multivariate Statistical Theory*. New York: Wiley, 1982.

[11] S. Haykin, *Adaptive Filter Theory*, 3rd ed. Englewood Cliffs, NJ: Prentice-Hall, 1996.

[12] N. L. Johnson, S. Kotz, and N. Balakrishnan, *Continuous Univariate Distributions, Volume 2*. New York: Wiley, 1995.

[13] R. Butler and M. Paolella, "Calculating the density and distribution function for the singly and doubly noncentral f," *Statist. Computing*, vol. 12, no. 1, 2002.

Alberto Rodríguez-Rivera (S'92) was born in Mayaguez, Puerto Rico in 1969. In 1992, he received B.S. degrees with honors (*Magna Cum Laude*) both in electrical engineering and computer engineering from the University of Puerto Rico-Mayaguez (UPRM). In 1995, he received the M.S. degree in electrical engineering also from the UPRM. Since then, he has been involved in several independent entrepreneurial projects and is currently pursuing the Ph.D. degree in electrical engineering from the University of Wisconsin-Madison.

His research interests include multidimensional, array, and statistical signal processing and its biomedical applications.

Barry D. Van Veen (S'81–M'86–SM'97–F'02) was born in Green Bay, WI. He received the B.S. degree from Michigan Technological University, Houghton, in 1983 and the Ph.D. degree from the University of Colorado, Boulder, in 1986, both in electrical engineering. He was an ONR Fellow while working on the Ph.D. degree.

In the spring of 1987, he was with the Department of Electrical and Computer Engineering at the University of Colorado. Since August of 1987, he has been with the Department of Electrical and Computer Engineering at the University of Wisconsin-Madison where he is currently a Professor. His research interests include signal processing for sensor arrays, nonlinear systems, adaptive filtering, wireless communications, and biomedical applications of signal processing. He co-authored, with S. Haykin *Signals and Systems*, 2nd ed. (New York: Wiley, 2002).

Dr. Van Veen was a recipient of a 1989 Presidential Young Investigator Award from the National Science Foundation and a 1990 IEEE Signal Processing Society Paper Award. He served as an associate editor for the IEEE TRANSACTIONS ON SIGNAL PROCESSING and on the IEEE Signal Processing Society's Technical Committee on Statistical Signal and Array Processing from 1991 through 1997 and is currently a member of the Sensor Array and Multichannel Technical Committee. He received the Holdridge Teaching Excellence Award from the ECE Department at the University of Wisconsin in 1997.

Ronald T. Wakai was born in East Orange, NJ, in 1958. He received the B.A. degree with honors in physics from Cornell University, Ithaca, NY, in 1980 and the Ph.D. degree in physics from the University of Illinois, Urbana, in 1987.

Since then, he has been with the Department of Medical Physics at the University of Wisconsin, Madison, WI, where he is currently a Professor. His research interests include basic and technical aspects of fetal biomagnetism and adult MEG.